NeuroImage: Clinical 28 (2020) 102433

Contents lists available at ScienceDirect

NeuroImage: Clinical

journal homepage: www.elsevier.com/locate/ynicl

High-resolution metabolic imaging of high-grade gliomas using 7T-CRT-FID-MRSI

Gilbert Hangel[a,b,*], Cornelius Cadrien[a,b], Philipp Lazen[a], Julia Furtner[c], Alexandra Lipka[a,d], Eva Hečková[a], Lukas Hingerl[a], Stanislav Motyka[a], Stephan Gruber[a], Bernhard Strasser[a,e], Barbara Kiesel[b], Mario Mischkulnig[b], Matthias Preusser[f], Thomas Roetzer[g], Adelheid Wöhrer[g], Georg Widhalm[b], Karl Rössler[b], Siegfried Trattnig[a,d], Wolfgang Bogner[a]

[a] High-field MR Center, Department of Biomedical Imaging and Image-guided Therapy, Medical University of Vienna, Vienna, Austria
[b] Department of Neurosurgery, Medical University of Vienna, Vienna, Austria
[c] Division of Neuroradiology and Musculoskeletal Radiology, Department of Biomedical Imaging and Image-guided Therapy, Medical University of Vienna, Vienna, Austria
[d] Christian Doppler Laboratory for Clinical Molecular MR Imaging, Vienna, Austria
[e] Athinoula A. Martinos Center for Biomedical Imaging, Department of Radiology, Massachusetts General Hospital, Harvard Medical School, Boston, MA, USA
[f] Division of Oncology, Department of Inner Medicine I, Medical University of Vienna, Vienna, Austria
[g] Division of Neuropathology and Neurochemistry, Department of Neurology, Medical University of Vienna, Vienna, Austria

ARTICLE INFO

Keywords:
Magnetic resonance spectroscopic imaging
High-grade glioma
7 Tesla
Concentric circle trajectories
Metabolic imaging
Glycine

ABSTRACT

Objectives: Successful neurosurgical intervention in gliomas depends on the precision of the preoperative definition of the tumor and its margins since a safe maximum resection translates into a better patient outcome. Metabolic high-resolution imaging might result in improved presurgical tumor characterization, and thus optimized glioma resection. To this end, we validated the performance of a fast high-resolution whole-brain 3D-magnetic resonance spectroscopic imaging (MRSI) method at 7T in a patient cohort of 23 high-grade gliomas (HGG).

Materials and methods: We preoperatively measured 23 patients with histologically verified HGGs (17 male, 8 female, age 53 ± 15) with an MRSI sequence based on concentric ring trajectories with a 64 × 64 × 39 measurement matrix, and a 3.4 × 3.4 × 3.4 mm^3 nominal voxel volume in 15 min. Quantification used a basis-set of 17 components including N-acetyl-aspartate (NAA), total choline (tCho), total creatine (tCr), glutamate (Glu), glutamine (Gln), glycine (Gly) and 2-hydroxyglutarate (2HG). The resultant metabolic images were evaluated for their reliability as well as their quality and compared to spatially segmented tumor regions-of-interest (necrosis, contrast-enhanced, non-contrast enhanced + edema, peritumoral) based on clinical data and also compared to histopathology (e.g., grade, IDH-status).

Results: Eighteen of the patient measurements were considered usable. In these patients, ten metabolites were quantified with acceptable quality. Gln, Gly, and tCho were increased and NAA and tCr decreased in nearly all tumor regions, with other metabolites such as serine, showing mixed trends. Overall, there was a reliable characterization of metabolic tumor areas. We also found heterogeneity in the metabolic images often continued into the peritumoral region. While 2HG could not be satisfyingly quantified, we found an increase of Glu in the contrast-enhancing region of IDH-wildtype HGGs and a decrease of Glu in IDH1-mutant HGGs.

Conclusions: We successfully demonstrated high-resolution 7T 3D-MRSI in HGG patients, showing metabolic differences between tumor regions and peritumoral tissue for multiple metabolites. Increases of tCho, Gln

Abbreviations: 2HG, 2-hydroxyglutarate; CE, contrast-enhanced; tCho, choline-containing compounds; tCr, total creatine, creatine + phosphocreatine; CRLB, Cramér–Rao lower bound; CRT, concentric ring trajectories; Ctn, cystathionine; Cys, cysteine; FID, free induction decay; FLAIR, fluid-attenuated inversion recovery; FOV, field of view; FWHM, full width at half maximum; GABA, γ-aminobutyric acid; Gln, glutamine; Glu, glutamate; Gly, glycine; GM, gray matter; GSH, glutathione; HGG, high-grade glioma; IDH, isocitrate dehydrogenase; mIns, (myo-)inositol; iMUSICAL, interleaved multichannel spectroscopic data combined by matching image calibration data; MM, macromolecules; MP2RAGE, magnetization-prepared 2 rapid acquisition gradient echoes; MRSI, magnetic resonance spectroscopic imaging; NAA, N-acetyl-aspartate; NAAG, N-acetyl-aspartyl glutamate; NAWM, normal-appearing white matter; NCE, non-contrast-enhanced; NEC, necrotic; PET, positron emission tomography; PT, peritumoral; ROI, region of interest; SAR, specific absorption rate; Ser, serine; SNR, signal-to-noise ratio; SVS, magnetic resonance single-voxel spectroscopy; T1w, T1-weighted; T2w, T2-weighted; Tau, taurine; TE, echo time; TME, tumor microenvironment; TR, repetition time; UHF, ultra-high-field; VOI, volume of interest; WET, water suppression enhanced through T_1 effects; WM, white matter; WT, wildtype

* Corresponding author at: Department of Neurosurgery, Medical University of Vienna, Vienna, Austria.
E-mail address: gilbert.hangel@meduniwien.ac.at (G. Hangel).

https://doi.org/10.1016/j.nicl.2020.102433
Received 8 May 2020; Received in revised form 8 September 2020; Accepted 9 September 2020
Available online 15 September 2020

(related to tumor metabolism), Gly (related to tumor proliferation), as well as decreases in NAA, tCr, and others, corresponded very well to clinical tumor segmentation, but were more heterogeneous and often extended into the peritumoral region.

1. Introduction

Research on the biochemistry of brain tumors has yielded insights into powerful onco-markers such as 2-hydroxygluarate (2HG), a product of mutated isocitrate-dehydrogenase (Yan et al., 2009), or glutamine (Gln) which has a major role in tumor metabolism (Altman et al., 2016). Those markers have increased our understanding of tumor metabolism beyond the involvement of glucose, lactate, and the Warburg effect (Potter et al., 2016) (i.e., tumor cells exhibit glycolysis over oxidative phosphorylation even in the presence of oxygen). However, *in vivo* detection or even imaging of such biochemical compounds and metabolites remains challenging. Single voxel proton magnetic resonance spectroscopy (SVS) has large voxel volumes, signal contamination by surrounding tissue, poor brain coverage, and the number of quantifiable metabolites is low. Magnetic resonance imaging (MRI) can only indirectly detect changes in metabolism (Stadlbauer et al., 2018) and positron emission tomography (PET) requires specific tracers. Mass and Raman spectroscopy (Fatou et al., 2016; St-Arnaud et al., 2018), as well as immunohistochemical and molecular-pathological methods cannot be used preoperatively. Magnetic resonance spectroscopic imaging (MRSI) can image biochemical changes of interest preoperatively, but has historically suffered from even more limitations than SVS. In clinical practice (1.5T and 3T), it is limited to low spatial resolutions, constricted by rectangular selection boxes and limited to a few metabolites. Usually, only total choline (tCho), total creatine (tCr) and total N-acetyl-aspartate (tNAA) can be quantified and cannot be further chemically separated (e.g., tNAA is the sum of NAA and N-acetylaspartylglutamic acid (NAAG)). Ultra-high-field (UHF) MR systems (e.g., 7T) improve the chemical specificity and signal-to-noise ratio (SNR), but technical limitations are imposed by increased specific absorption rates (SAR), B_0- and B_1-inhomogeneities, and fast T_2* relaxation (Moser et al., 2012). Nevertheless, promising metabolic imaging of gliomas with reliable differentiation of glutamate (Glu) and Gln has been demonstrated (Li et al., 2015), although with low spatial resolution. Yet, this differentiation was not possible at $\leq$3T, where the mix of Gln and Glu was thus denoted Glx.

Over the course of the last decade, a different approach for MRSI acquisition, based on the direct acquisition of the free-induction-decay (FID) signal, was proposed (Bogner et al., 2020; 2012;; Gruber et al., 2017; Henning et al., 2009) that is less affected by these issues. The most important feature of FID-MRSI is the outstanding boost in SNR for J-coupled metabolites, such as Gln, Glu, my-Inositol (mIns), and taurine (Tau). FID-MRSI was then further refined to allow accelerated high-resolution coverage without a selection box but still for only a few slices (Hangel et al., 2016; Strasser et al., 2017). The first promising results of this high-resolution MRSI approach were shown in gliomas recently (Hangel et al., 2019). Exchanging the previously used conventional phase-encoding with a non-Cartesian, concentric ring trajectory-based image readout (Hingerl et al., 2019) allowed for a further jump in acquisition speed. This has finally enabled rapid whole-brain FID-MRSI and indicated that mIns and Glycine (Gly) – additional markers for tumor proliferation (Kim et al., 2015) – can be potentially separated in brain tumors. These metabolites were previously suggested as prognostic markers for the patient's overall survival (Mörén et al., 2015).

By acquiring additional information in comparison to clinical routine protocols, the preoperative definition of the tumor margins of high-grade gliomas might be improved. By improved presurgical tumor characterization, we expect to optimize in future glioma resections resulting in enhanced patient prognosis. Overall, we assume that the 7T fast high-resolution whole-brain 3D-MRSI technique is a promising candidate for preoperative metabolic *in vivo* imaging of high-grade gliomas.

Table 1
Overview table of patients including histopathological diagnosis, immunohistochemical and molecular-pathological markers and an overview of 7T MRSI measurement quality, tCr-based voxel quality rejection and the rejection of patient datasets from further analysis.

Patient	Age at Measurement [y]	Sex	Histophatological diagnosis (WHO 2016)	Grade (WHO 2016)	IDH-mutation	MGMT Methylation	Qualitative evaluation	Voxel rejection in ROI	Status
1	51	m	Glioblastoma, IDH-mut	4	IDH1	Methylated	Good	18%	Accepted
2	52	m	Glioblastoma, IDH-mut	4	IDH1	Methylated	Good	6%	Accepted
3	47	f	Glioblastoma, IDH-WT	4	WT	Unmethylated	Acceptable	26%	Accepted
4	46	f	Anaplastic Astrocytoma, IDH-mut	3	IDH1	Methylated	Good	8%	Accepted
5	29	m	Anaplastic Astrocytoma, IDH-mut	3	IDH1	Methylated	Good	24%	Accepted
6	52	m	Glioblastoma, IDH-WT	4	WT	Methylated	Good	19%	Accepted
7	58	m	Glioblastoma, IDH-WT	4	WT	Unmethylated	Bad, low position	39%	Rejected
8	34	f	Anaplastic Astrocytoma, IDH-WT	3	WT	Methylated	Good	6%	Accepted
9	71	m	Glioblastoma, IDH-WT	4	WT	Methylated	Good	6%	Accepted
10	75	f	Glioblastoma, IDH-WT	4	WT	Methylated	Bad, low position	46%	Rejected
11	65	f	Anaplastic Astrocytoma, IDH-WT	3	WT	Unmethylated	Good	8%	Accepted
12	51	m	Anaplastic Oligodendroglioma, IDH-mut	3	IDH1	Methylated	Acceptable	14%	Accepted
13	62	m	Anaplastic Astrocytoma, IDH-mut, Recurrence	3	IDH1	Methylated	Bad, low position	56%	Rejected
14	30	f	Glioblastoma, IDH-WT	4	WT	Methylated	Good	2%	Accepted
15	34	m	Anaplastic Astrocytoma, IDH-mut	3	IDH1	Methylated	Good	19%	Accepted
16	56	m	Anaplastic Oligodendroglioma, IDH-mut, Recurrence	3	IDH1	Methylated	Good	11%	Accepted
17	61	m	Glioblastoma, IDH-WT	4	WT	Methylated	Acceptable	31%	Accepted
18	60	m	Glioblastoma, IDH-WT, Recurrence	4	WT	Methylated	Acceptable	11%	Accepted
19	77	m	Glioblastoma, IDH-WT, Recurrence	4	WT	Unmethylated	Acceptable	27%	Accepted
20	28	f	Anaplastic Astrocytoma, IDH-mut	3	IDH1	Methylated	Good	22%	Accepted
21	62	m	Glioblastoma, IDH-WT, Recurrence	4	WT	Methylated	Bad	35%	Rejected
22	77	f	Glioblastoma, IDH-WT	4	WT	–	Acceptable	22%	Accepted
23	46	m	Anaplastic Astrocytoma, IDH-mut	3	IDH1	–	Bad	30%	Rejected

1.1. Purpose

Consequently, the aim of our explorative study was to evaluate the potential of whole-brain FID-MRSI at 7T to reliably and simultaneously image a comprehensive neurochemical profile in 23 high-grade gliomas (HGGs), including major markers of onco-metabolism and proliferation, such as NAA, tCr, tCho, Glu, Gln, mIns, and Gly.

2. Methods

2.1. Subject recruitment and clinical measures

This study was conducted in accordance with the Declaration of Helsinki and with approval of the institutional review board. Written, informed consent was obtained from all participants. Patients with suspected brain tumors, no contraindications for 7T MRI (e.g., claustrophobia, ferromagnetic implants, non-ferromagnetic metal head implants > 12 mm, and pregnancy) and a Karnofsky performance status > 70 were recruited by the Departments of Neurosurgery and Oncology prior to therapy/surgery. Of 48 patients prospectively measured between November 2018 and December 2019, 23 patients with histologically verified HGGs (15 male, 8 female, age 53 ± 15, histopathological diagnosis by the Division of Neuropathology and Neurochemistry according to the latest WHO classification of 2016 (Louis et al., 2016) as in Table 1) were included in this study. All patients were measured before treatment (i.e. resection, radiotherapy, chemotherapy), in case of the five patients with recurrent tumors (Table 1), this means before treatments after recurrence was suspected. Preliminary results for patient #1 were published in (Hingerl et al., 2019).

The 7T MRSI study protocol was acquired after a routine clinical 3T MRI protocol (Mert et al., 2015) including at least T2-weighted imaging (T2w), fluid-attenuated inversion recovery (FLAIR), and T1-weighted imaging (T1w) before and after contrast agent administration (Gadoteridol, 0.1 mmol/kg).

2.2. 7T MRSI measurement protocol

We performed the study protocol using a 7T whole-body-MR imager (Magnetom, Siemens Healthcare, Erlangen, Germany) equipped with a 32-channel receive coil array (Nova Medical, Wilmington, MA, USA) and a gradient system with a 70 mT/m maximum gradient strength per direction and a 200 mT/m/s nominal slew rate. In addition to MRSI, it included B_1^+-maps for flip-angle optimization, as well as morphological reference imaging: Magnetization prepared 2 rapid gradient echoes (MP2RAGE) for T1-weighted MRI (TR 5000 ms, TE 4.13 ms, TI_1 700 ms, TI_2 2700 ms, 0.8 × 0.8 × 0.8 mm^3 resolution, 8:02 min with GRAPPA factor 3), and fluid-attenuated inversion recovery (FLAIR) for T2-weighted MRI (TR 8000 ms, TE 270 ms, TI 2180 ms, 0.8^3 mm^3 isotropic resolution, 8:10 min with GRAPPA factor 3).

The fast high-resolution whole-brain 3D-MRSI sequence (Hingerl et al., 2019) used 2D-concentric ring trajectories (CRTs) and through-plane phase encoding to cover a field of view (FOV) of 220 × 220 × 133 mm^3 with a volume of interest (VOI) of 220 × 220 × 85 mm^3 and a 64 × 64 × 39 measurement matrix, corresponding to 3.4 × 3.4 × 3.4 mm^3 nominal resolution. The FID acquisition was performed following a 39° Ernst flip angle (i.e., optimized for the average T_1 of NAA, Cr, and Cho) with an acquisition delay of 1.3 ms. With a TR of 450 ms and 7T-optimized WET water suppression (Hangel et al., 2016; Ogg et al., 1994), an SNR-optimized readout of 345 ms duration and a 2778 Hz spectral bandwidth was possible. With one average and variable temporal interleaves, the MRSI scan had a duration of 15:00 min.

The FOV was placed so that the entirety of the morphologically visible tumor and the cerebrum was covered as well as possible and oriented in parallel to the corpus callosum.

2.3. Data processing

Offline MRSI data processing utilized an in-house-developed software pipeline (Považan et al., 2014) consisting of Matlab (R2013a, MathWorks, Natick, MA, USA), Bash (v4.2.25, Free Software Foundation, Boston, MA, USA), and MINC (MINC tools, v2.0, McConnell Brain Imaging Center, Montreal, QC, Canada). Data processing included an iMUSICAL coil combination (Hingerl et al., 2018; Moser et al., 2019; Strasser et al., 2013) and water normalization similar to (Maudsley et al., 2009), k-space reconstruction with in-plane convolution gridding (Hingerl et al., 2018), spatial Hamming filtering, channel-wise noise-decorrelation, off-resonance correction, and lipid signal removal using L2-regularization (Bilgic et al., 2013).

Lacking the local T1 relaxation times for metabolites and intratumoral water concentrations, we could not calculate concentration estimates. The resultant voxel spectra were instead quantified as institutional units using LCModel (v6.3-1, LCMODEL Inc, ONT, CA) with a basis set that included NAA, NAAG, Cr, phosphocreatine, phosphocholine, glyceryl-phosphorylcholine , mIns, scyllo-Ins, γ-aminobutyric acid (GABA), glutathione (GSH), Glu, Gln, Gly, Tau, cystathionine (Ctn), cysteine (Cys), serine (Ser), 2HG, and a macromolecular background (Považan et al., 2015) with an evaluation range of 0.2-1.2 ppm and 1.8-4.2 ppm (excluding the lipid resonance at 1.3 ppm). In order to evaluate the reliability of the separation of Gly/mIns and Gln/Glu, we created a simulation model (see Supplement 1 for details).

3D images for every metabolite were created from the results of the spectral quantification. These images were masked based on the quality criteria described in 2.4 and tricubically interpolated for display purposes.

Preoperative, clinical, T1-weighted (native and contrast-enhanced), T2-weighted and FLAIR images were skull-stripped and co-registered via FSL (FMRIB Software Library v5.0, Oxford, UK) to the 7T images. All HGGs were segmented by an experienced neuroradiologist (J.F.) using only these co-registered clinical MRI datasets into regions of interest (ROIs) for the following different tumor compartments (i.e., non-enhancing or edema (NCE); contrast-enhancing (CE); and necrosis (NEC)). The peritumoral region (PT) adjacent to the tumor segmentation, defined as coherent changes starting in or at the border of the segmented ROIs, was also included for data evaluation.

2.4. Data evaluation

Spectral quality (i.e., signal-to-noise ratio (SNR) calculated using the pseudo-replica method and full-width-at-half-maximum (FHWM) of tCr at 3.02 ppm) and fitting quality (i.e., Cramér–Rao lower bounds (CRLB) of all metabolites) were calculated voxel-wise. Based on these, spectra with insufficient quality (i.e., at least one of these: tCr SNR < 5; tCr FWHM > 0.15 ppm; metabolite CRLB > 40 %; metabolite fit value > 13 median absolute deviations) in both brain and tumor tissue were excluded from metabolic image generation and further analysis. The fraction of rejected voxels within the segmented tumor ROIs was assessed.

The quality of metabolic images was also assessed qualitatively by two readers in consensus (G.H., C.C.). We evaluated the resultant metabolic images for overall quality and artifacts per patient as well as overall image quality per metabolite. Individual metabolic images were rejected if the majority of voxels was outside the defined quality criteria and if no coherent image structure in normal-appearing brain tissues or tumor was visible. Patient datasets were rejected if more than one-third of voxels in the ROI failed the quality test. Rejected patient datasets were excluded from further evaluation. The images of metabolites that were rejected in the majority of cases were also excluded from further evaluation for all patients. Mean CRLBs + standard deviation as a quality control for spectral separation of the Glu/Gln, mIns/Gly and NAA/NAAG pairs were calculated. In total, the evaluation reliability of individual metabolite quantification results was based on voxel quality

measures as defined above, reader assessment and presence of image artifacts.

Due to the small cohort and heterogeneous sample of different HGGs, no statistical comparison of metabolite concentrations or ratios was attempted. Instead, the remaining metabolic images were first evaluated qualitatively with respect to metabolite changes (i.e., trends of increase, decrease, mix of increase/decrease, and no change compared to normal-appearing brain tissue) without considering the tumor segmentation. This qualitative evaluation was then repeated with more detailed spatial and trend criteria to emphasize the capabilities of MRSI. Within the segmented tumor ROIs and the PT more gradual trends of increase, mostly increase, decrease, mostly decrease, mix of increase/decrease, no change within the selected ROI compared to normal-appearing brain tissue were investigated. The resultant metabolic trends were compared to the findings from histopathology (grade, IDH mutation status, MGMT methylation) and analyzed for different metabolic profiles between the tumor types.

3. Results

3.1. MRSI Quality

Overall, 21% of all voxels within the segmented tumor ROIs were discarded, which resulted in five of the 23 patient measurements being discarded based on the rejection criteria (Table 1). These five datasets were also rated as unusable in general quality and included three cases of basal locations with a challenging shim at 7T and two cases of cranial metal implants from previous surgery. No technical/methodological problems were recorded for these five cases. Of the included 18 patient measurements, 12 were of good and six of acceptable overall quality. These 18 cases included 9 IDH-mutant and 9 IDH-WT gliomas. According to the WHO grade, 10 grade 4, and 8 grade 3 cases were diagnosed. Younger patients showed overall better data quality (all patients under 46 were rated as good; median patient age of the 18 accepted measurements: 51 years [28-77 range]; median patient age of the five rejected measurements: 62 years [46-75 range]).

Our simulation model confirmed that for the SNR and FWHM found in our tumors, a reliable separation of Gly/mIns and Gln/Glu was indeed possible (Sup. Figs.1 and 2). Especially for the red box signifying LCModel SNRs between 4 and 9 and FWHMs between 0.04 and 0.06 ppm, corresponding to the range of SNRs and FWHMs found in our tumor segmentations, the metabolite concentrations in question are in the range of 30% of the ground truth (see Supplement 1 for details).

Of the quantified metabolites, NAA, NAAG, tCho, tCr, Glu, Gln, mIns, Gly, Ser, and GABA were successfully fitted in all 18 patients, while Tau, Ctn, Cys and GSH were acceptable in most cases (Table 2). Asp was not satisfyingly quantified, in general, as well as 2HG, for which there was no clear difference between the IDH1 mutant and wildtype tumors. Mean CRLBs + standard deviation were, for Gln, 22 ± 18% within the tumor segmentation and 30 ± 20% within the rest of the brain mask ; corresponding CRLBS were 17 ± 15% and 14 ± 14% for Glu; 23 ± 18% and 18 ± 16% for mIns; 44 ± 20% and 52 ± 20% for Gly; 28 ± 21% and 29 ± 22% for NAAG and 16 ± 17% and 12 ± 16% for NAA. Supplementary figure 3 displays that within hotspots, CRLBs are notably lower than over the whole segmentation.

As shown in the sample spectra (Fig. 1), regional spectral differences were found between tumor regions and healthy-appearing brain tissue. In 13 patients, there was a strong intra-tumoral heterogeneity. In general, our high-resolution metabolic images showed strong spatial heterogeneity for various metabolites, with regions of increased and decreased metabolite levels that are summarized in Table 2. The metabolic images of two patients presented in Fig. 2 illustrate these findings.

3.2. Comparison to tumor segmentation

A more detailed analysis of metabolic images within the segmented ROIs based on conventional structural imaging shows more distinct findings: Gln, Gly and tCho were increased and NAA and tCr were decreased in nearly all tumor regions and patients. Examples for this are an increase or partial increase (of a total of 10 NEC, 13 CE, and 17 NCE ROIs) of tCho in 13 CE and 15 NCE ROIs, an increase or partial increase of Gln in 13 CE and 15 NCE ROIs, an increase or partial increase of Gly in 13 CE and 16 NCE ROIs, a decrease or partial decrease of NAA in 13 CE and 17 NCE ROIs, and a decrease or partial decrease of NAA in 13 CE and 14 NCE ROIs (full overview in Fig. 3). Tau was mostly increased (e.g., increases or partial increases in 11 of the CE and 14 of the NCE regions), Ser showed mixed trends over all regions (e.g., increases in six and decreases in seven of the CE regions), NAAG and Cys were increased in the CE-region compared to the NCE-region, and Ctn was increased in NCE compared to CE.

Our results for tCho, Gln and Gly were found to be the most consistent as markers for activity in MRI-visible tumors and beyond, as presented per patient and segmented region in Table 3. We found the imaging of Gly (Fig. 4) to be of special interest as a metabolic marker,

Table 2
Summary of a qualitative evaluation of metabolite trends over all patient measurements of sufficient quality and all metabolites. Symbols: + = overall increase in the glioma; − = overall decrease in the glioma; 0 = no difference from surrounding tissue; +− = regions of increase and decrease; n.Q.: not quantifiable

Patient	Hist. Diagnosis	Grade	IDH	NAA	NAAG	tCho	tCr	Glu	Gln	mIns	Gly	Tau	Ser	Cys	Ctn	GABA	GSH
1	Glioblastoma, IDH-mut	4	IDH1	−	+	+−	−	+−	+−	+−	+	+−	−	n.Q.	+−	+−	+−
2	Glioblastoma, IDH-mut	4	IDH1	−	+	+	−	−	+−	−	+	+−	+−	+−	−	+−	−
3	Glioblastoma, IDH-WT	4	WT	−	−	+−	−	−	+−	−	+	n.Q.	+−	n.Q.	+	−	+−
4	Anaplastic Astrocytoma, IDH-mut	3	IDH1	−	+	+	+−	−	+	+−	+	+−	+−	+−	+	+−	+
5	Anaplastic Astrocytoma, IDH-mut	3	IDH1	−	+−	+	−	+−	+−	+−	+−	n.Q.	+−	+−	+	+−	+−
6	Glioblastoma, IDH-WT	4	WT	−	+−	+−	−	+−	+	−	+	+−	+	n.Q.	+	+−	+−
8	Anaplastic Astrocytoma, IDH-WT	3	WT	−	+−	+−	+−	+−	−	+−	+−	+−	+−	+	+−	+−	+−
9	Glioblastoma, IDH-WT	4	WT	−	+−	+−	+−	+−	+	+−	+−	+−	+−	−	+	+−	+−
11	Anaplastic Astrocytoma, IDH-WT	3	WT	+−	+	+−	+	+−	+	+	+	+	+−	+	+	+−	+
12	Anaplastic Oligodendroglioma, IDH-mut	3	IDH1	−	+−	+	+−	−	+−	−	+−	+	+−	+−	+−	+−	+−
14	Glioblastoma, IDH-WT	4	WT	+−	+−	+	+−	−	+	+−	+	+	+−	+	n.Q.	+−	+
15	Anaplastic Astrocytoma, IDH-mut	3	IDH1	−	+−	+	−	+−	+	+−	+−	+	+−	n.Q.	+−	+−	+−
16	Anaplastic Oligodendro-glioma, IDH-mut, Recurrence	3	IDH1	−	+−	+−	+−	+−	+−	−	+−	+−	−	0	+−	+−	+−
17	Glioblastoma, IDH-WT	4	WT	+−	+−	+	+−	+−	+	+−	+−	+−	+−	+−	n.Q.	+−	+−
18	Glioblastoma, IDH-WT, Recurrence	4	WT	−	−	+−	+−	−	+	−	+−	+−	+−	+−	n.Q.	+−	−
19	Glioblastoma, IDH-WT, Recurrence	4	WT	−	+−	+	+−	+−	+	−	+−	+−	+−	+−	n.Q.	+−	n.Q.
20	Anaplastic Astrocytoma, IDH-mut	3	IDH1	−	+−	+	+−	−	+	+−	+−	+−	+−	−	+	+−	+−
22	Glioblastoma, IDH-WT	4	WT	−	−	+−	+−	+−	+	−	+−	+−	+	+−	+	+−	n.Q.

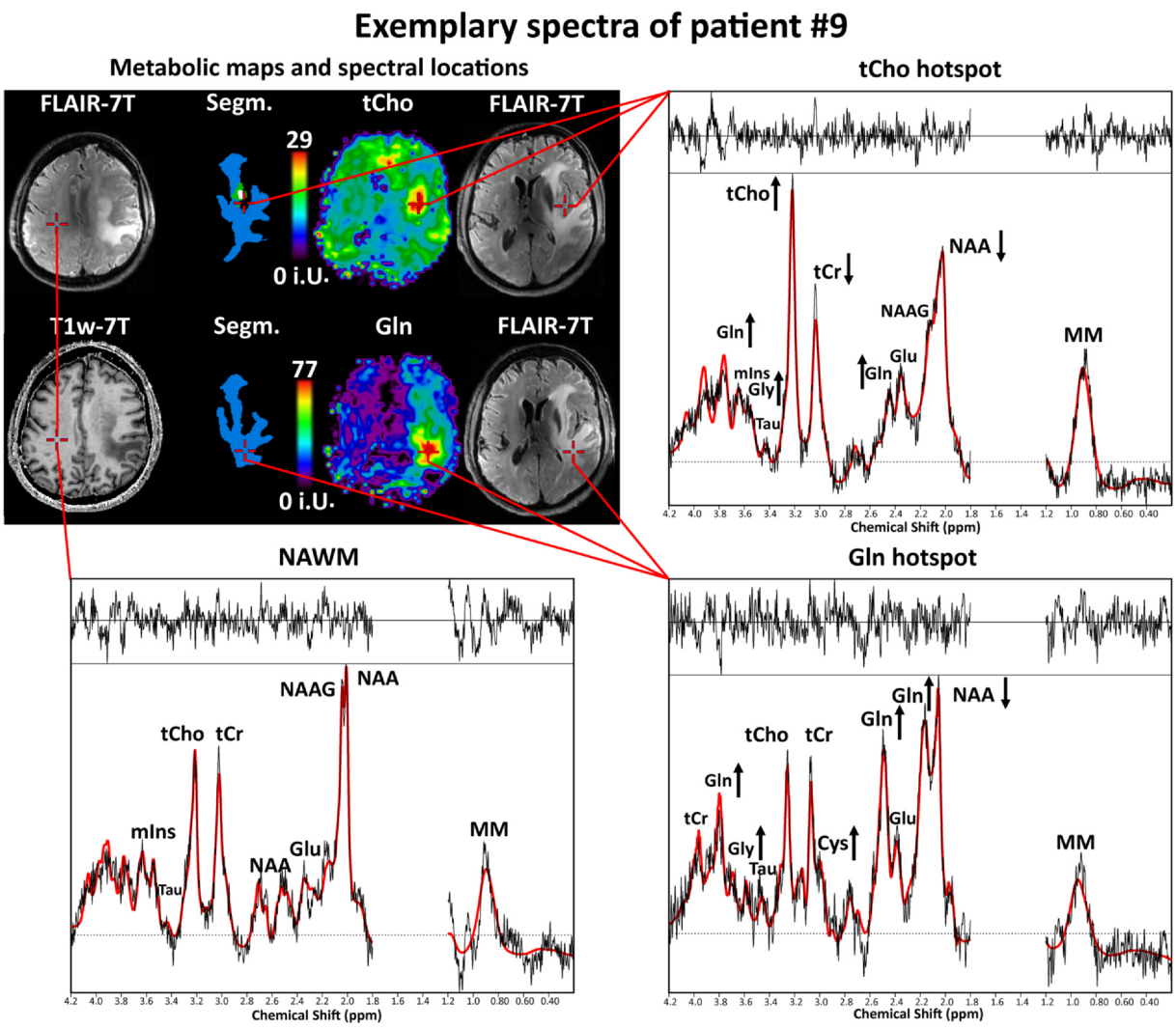

Fig. 1. Example spectra of two tumor voxels and one NAWM voxel of patient #9. Different metabolic patterns between a tCho and a Gln hotspot are visible. The spectra were phased for display purposes.

separable from mIns and showing regions of enhancement similar to the established marker tCho and the recently investigated Gln (Fig. 5). The benefits of the possible separation of mIns and Gly, as well as Gln and Glu at 7T, are shown in Fig. 6.

3.3. Comparison to histopathology

While 2HG could not be satisfyingly quantified, there was a trend toward increased Glu in the CE region of IDH-wildtype tumors and of decreased Glu in IDH-mutant tumors. WHO grade 4 cases appeared to have a more prominent decrease in mIns than WHO grade 3 cases that showed a more mixed behavior. Furthermore, we found reduced GSH and increased Glu in non-contrast-enhancing grade 4 regions. Fig. 5 shows sample metabolic images in relation to the segmentations.

4. Discussion

We successfully demonstrated that it is possible to reliably acquire high-resolution, whole-brain metabolic images in 18 out of 23 HGG patients using our FID-MRSI sequence at 7T. We acquired detailed 3D-metabolic images for multiple metabolites that could allow an unprecedented preoperative evaluation of tumor biomarkers, such as tCho or Gln. The data obtained in five additional patients had to be excluded mainly because of artifacts related to implants or the tumor location too basally located in the brain. In the latter cases, the second-order B_0-shims were most likely not able to provide sufficiently high B_0 homogeneity. We, therefore, argue that, under the limitations with regard to tumor location and implants, our method performed robustly in the vast majority of cases, with more extensive measurement series likely to succeed. CRLBs as measure for fitting reliability for metabolites of interest like Gln and Gly were satisfactorily low within hotspots (Sup.Fig.3) and remained acceptable even over the whole, often heterogeneous, tumors. Whit our spectral simulations, we further demonstrated that our FID-MRSI approach can differentiate Gly from mIns and Gln from Glu at *in vivo* conditions, addressing concerns about possible misfitting of metabolites due to low signal quality. A deviation of up to 30% to the ground truth needs to be considered for any more elaborate quantification attempts, but for the current results that show intensity increases for Gly or Gln in the range of $\times$5-10, quantification accuracy is sufficient. As the results show that Gly and Gln can be expected to be under- and not overfitted with worse linewidth and SNR, better measurement quality can be expected to result in even more pronounced contrast on the resulting metabolic maps.

We showed significantly improved coverage and resolution compared to prior 7T MRSI of gliomas (Hangel et al., 2019; Li et al., 2015). The nominal voxel size of 0.039 cm^3 (64 $\times$ 64 $\times$ 39 matrix) outperformed even that of our previous single-slice glioma study (0.095 cm^3) (Hangel et al., 2019) and was acquired with 39 instead of 4

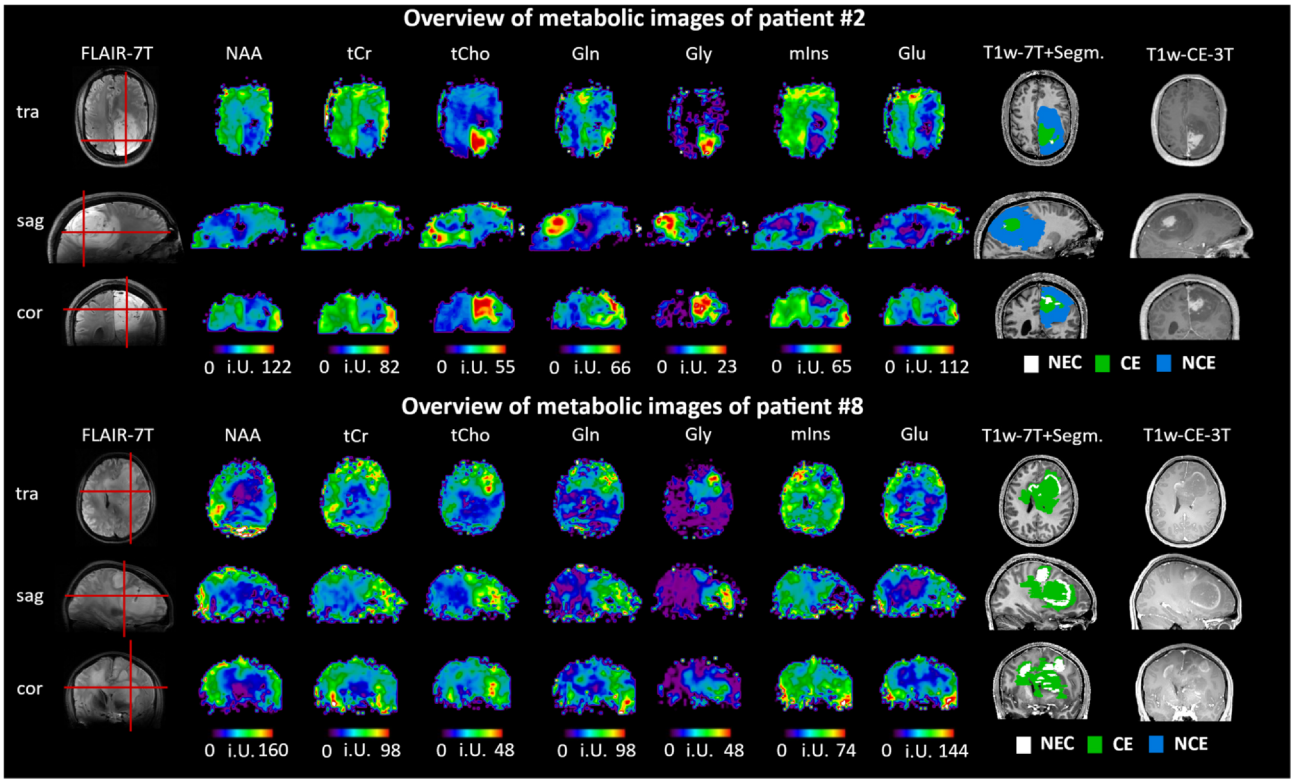

Fig. 2. Images of the most reliable metabolites of all primary orientations in patients #2 and #8. Next to the well-researched marker tCho, Gln and Gly also appear to coincide with tumor activity. The red reference lines indicate the positions of the displayed MRSI slices.

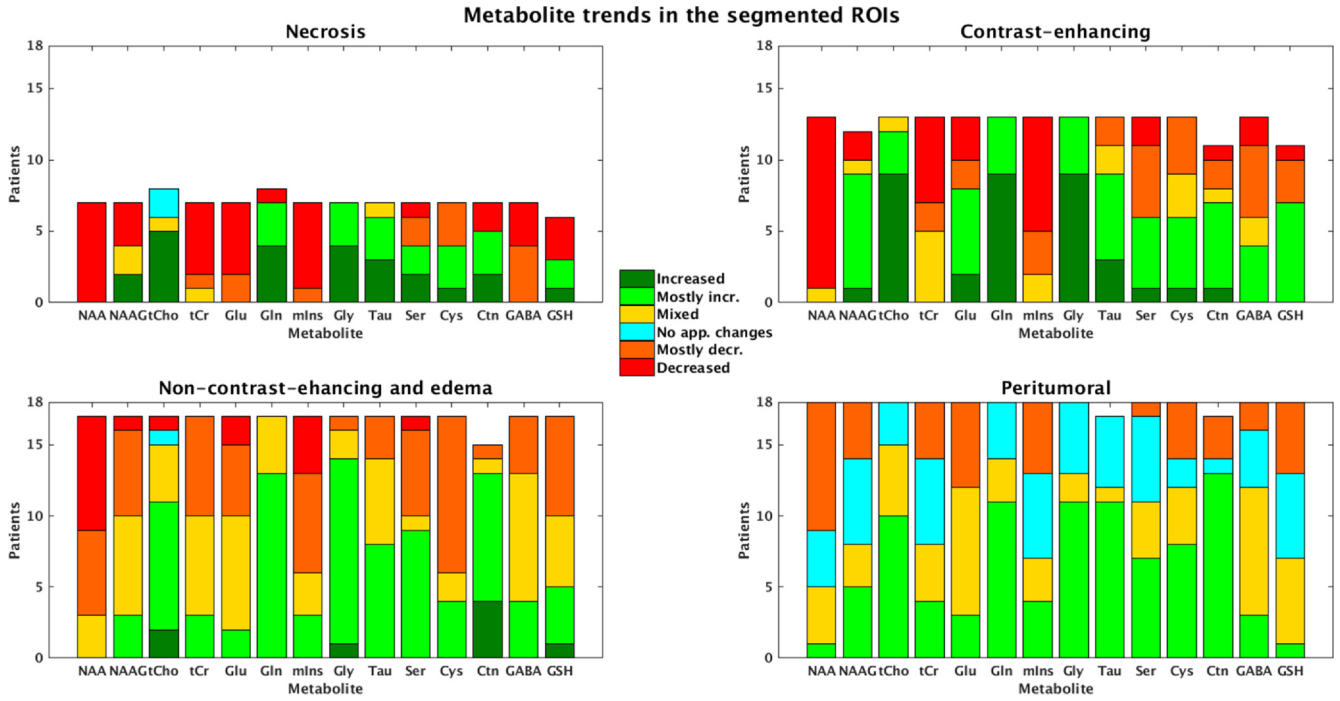

Fig. 3. Overview of qualitative trends of metabolic activity per ROI and metabolite. Different bar sizes are attributable to the fact that not all tumor ROIs were present in all cases, combined with the filtering of voxels outside of the defined quality criteria (which would, in some cases, result in a metabolite not being successfully quantified at all in a specific ROI). NEC was segmented, within the MRSI FOV and within the quality criteria in 10 of 18 patients, with CE and NCE respectively in 13 and 17 of the patients. Again, tCho, Gln, and Gly showed a clear overall increase within the segmented tumor region. Many other metabolites showed a mixed behavior and, in many cases, there was also increased metabolic divergence in the peritumoral region.

Table 3
Detailed metabolic trends for tCho, Gln, and Gly over the segmented ROIs for all patients. A strong similarity of changes in these three metabolites can be observed. Symbols: + = increased; +0 = mostly increased; +− = mix of increased and decreased; 0 = no observed difference; 0− = mostly decreased; − = decreased; n.s. = not segmented; excl. = excluded based on quality criteria.

Necrosis				Contrast-enhancing				Non-enhancing/edema				Peritumoral			
Pat	tCho	Gln	Gly	Pat	tCho	Gln	Gly	Pat	tCho	Gln	Gly	Pat	tCho	Gln	Gly
1	0	−	+−	1	+	+	+	1	n.s.	n.s.	n.s.	1	+0	+0	0
2	+	+0	+	2	+	+0	+	2	+−	+0	+0	2	+−	0	0
3	0	+0	+	3	+−	+0	+	3	+−	+−	+0	3	+−	+−	0
4	+	+	+	4	+	+	+	4	+	+0	+0	4	+0	0	+0
5	n.s.	n.s.	n.s.	5	n.s.	n.s.	n.s.	5	+0	+−	+0	5	+0	+0	+0
6	+−	+0	+	6	+0	+0	+	6	+0	+0	+0	6	+0	+0	0
8	n.s.	n.s.	n.s.	8	+0	+0	+0	8	+0	+0	+0	8	+0	+0	+0
9	+	+	+0	9	+	+	+0	9	+−	+0	+−	9	+−	+−	0
11	n.s.	n.s.	n.s.	11	n.s.	n.s.	n.s.	11	+0	+0	+	11	+0	+0	+0
12	n.s.	n.s.	n.s.	12	n.s.	n.s.	n.s.	12	+0	+0	+0	12	+0	+0	+0
14	n.s.	n.s.	n.s.	14	n.s.	n.s.	n.s.	14	+0	+0	+0	14	+0	+0	+0
15	n.s.	n.s.	n.s.	15	+	+	+	15	+0	+0	+−	15	+−	+0	+−
16	n.s.	n.s.	n.s.	16	+	+	+0	16	+0	+−	+0	16	0	+0	+0
17	+	+	excl.	17	+	+	+	17	+	+0	+0	17	+−	+0	+0
18	excl.	excl.	excl.	18	+	+	+	18	−	+0	0−	18	+0	0	+0
19	excl.	excl.	excl.	19	+	+	+0	19	+−	+0	+0	19	+0	+−	+0
20	n.s.	n.s.	n.s.	20	n.s.	n.s.	n.s.	20	+0	+0	+0	20	0	0	+−
22	+	+	+0	22	+0	+	+	22	0	+−	+0	22	0	+0	+0

slices in the same time(15 min total) with sufficient SNR. The smaller achieved voxel size reduces partial-volume effects and improves intra-voxel B_0-homogeneity, allowing better spatial and spectral separation of intratumoral heterogeneities than (Li et al., 2015). In comparison to our VOI of 22 × 22 × 8.5 cm^3, (Li et al., 2015) were limited to a 1 cm^3 resolution with a 20 × 22 × 8 matrix and suppression bands reducing the VOI acquired in 11 min. Our method has a larger slab thickness and produces whole-slice maps. In combination, the higher spatial resolution and extended brain coverage enable a more detailed and comprehensive metabolic characterization of tumor heterogeneity in HGGs compared to previous research. Our results corresponded well to tumor segmentation based on conventional clinical MRI, and even showed more detailed and heterogeneous hyperintense regions.

MRSI using common MRI devices has been demonstrated in many studies, but is usually restricted to tNAA, tCho, and tCr, if no dedicated approach to quantify other metabolites is used. Together with other clinical imaging techniques, these markers are often used for non-invasive tumor grading (Boonzaier et al., 2017; Bulik et al., 2013; Caulo et al., 2014; Wang et al., 2016) mostly via the ratio of tCho to tNAA (Stadlbauer et al., 2007; Wang et al., 2016). This is in agreement with our results. Previous 7T MRSI studies (Hangel et al., 2019; Li et al., 2015) report an increase of Gln in tumor tissue. 3T MRSI has found an increase in Gly from low- to high-grade gliomas (Maudsley et al., 2014). Our results confirm this finding, but show that the locations of tCho, Gln, and Gly hotspots do not always correspond spatially, which should be further investigated, as we currently do not understand the potential differences in tumor-microenvironments that may underlie this. As *in vivo* MRSI offers limited comparison possibilities for most of our findings, we instead compare our results with SVS, studies of glioma biochemistry and molecular pathology. Gln is a factor in multiple tumor characteristics, including metabolism, biosynthesis, homeostasis, expression of oncogenes, and can importantly act as an alternative carbon source rather than glucose in the tricarboxylic acid cycle (Altman et al., 2016). Gln has also been linked to mTOR kinase inhibitor resistance in glioblastomas (Tanaka et al., 2015). Our quantifiable metabolic range, without glucose and lactate, does not directly represent the Warburg effect, and therefore, cannot be used to differentiate different tumor micro-environments based on oxidative phosphorylation and glycolysis. But, as Gln appears to be the major carbon source for tumors in hypoxic conditions (Wise et al., 2011), it should be investigated in the context of these tumor-microenvironments. Gln imaging would also be an ideal control modality for glutamine-targeting therapies (Obara-Michlewska and Szeliga, 2020).

In *ex vivo* HR-magic-angle-spinning NMR studies that were able to separate Gly from mIns, an increase in Gly and a reduction of mIns were detectable in high-grade gliomas (Righi et al., 2010) compared to low grade gliomas, where both mIns and Gly increased. 3T MRS (Kallenberg et al., 2009) has found mIns and Gln increasing in suspected infiltration and astrocytosis, but was not designed to separately quantify mIns and Gly. It could be hypothesized that the progression from infiltration or lower grade to (hypoxic) GBM reduces the availability of the glial marker mIns, while Gln as important part of GBM biochemistry further increases in concentration. Ser, for which we found heterogeneous behavior, was previously successfully quantified in gliomas using SVS at 7T (Choi et al., 2009), in connection with Cys and Gly, and appears to be higher for faster tumor proliferation and correlates with tumor progression (Ganji et al., 2016; Mattaini et al., 2016). Future studies that include low- and high-grade gliomas could evaluate the use of Gly as a preoperative marker for grading and could verify the potential value of MRSI beyond the evaluation of tCho in tumors. Cys, which we found to be increased in the CE-region compared to the NCE region, is connected to GSH (McBean, 2017), which we found reduced in NCE grade 4 regions. Ctn, recently reported as detectable using SVS in IDH1-gliomas (Branzoli et al., 2019), was increased in NCE compared to CE. As NAAG is difficult to separate from NAA, we could not relate our finding of an increase in CE over NCE to previous research. Also, for taurine, which appears to present a GM/WM contrast in the healthy brain (Lei and Peeling, 2000), and which we found to be mostly increased in gliomas, related brain tumor studies are limited. In summary, more research is needed to confirm, test, and better comprehend our results.

While we could not satisfyingly quantify 2HG itself, the reliable quantification of which requires special efforts even at 7T (Berrington et al., 2018).Recent research has found a connection between glutamatergic synapses and tumor proliferation (Venkataramani et al., 2019) that further highlights the role of Glu in gliomas and demonstrates that it is not only necessary to separate Gln form Glu in order to understand glioma metabolism, but also to separate Glu from Gln activity to investigate the role of glutamatergic synapses in brain tumors. mIns seemed to decrease from Grade 3 to 4 in our study, whereas previous studies reported higher mIns levels for HGG than for low-grade glioma (Kallenberg et al., 2009). This disagreement could be related to the fact

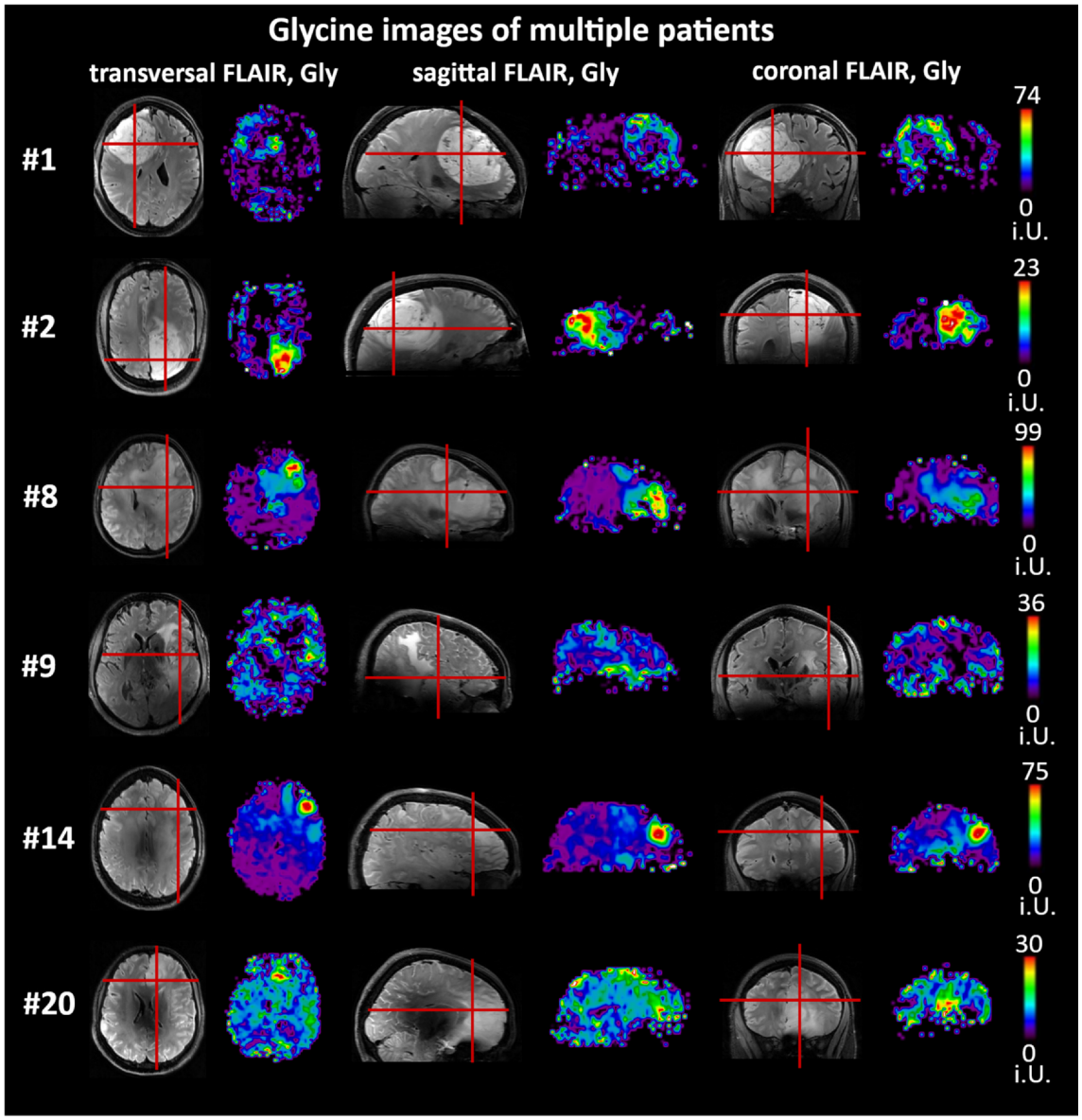

Fig. 4. Examples of glycine images over multiple patients show a good correspondence to morphological imaging and even more differentiated activity, as in patient #1. The red reference lines indicate the positions of the displayed MRSI slices.

that the separation of Gly and mIns was not directly possible in this previous study at 3T.

Searching for all these findings in a wider 7T MRSI database of gliomas could lead to metabolic profiles that reflect these metabolic changes in different tumor compartments.

Since the patient prognosis of high-grade gliomas depends mainly on the extent of resection, new imaging methods for precise pre-operative definition of the tumor margin are of major importance. Employing high-resolution metabolic imaging will support in future the neurosurgeon to better define the tumor margin in high-grade gliomas leading to improved extent of resection and thus patient prognosis. Targeted biopsies of metabolic hotspots can improve tumor grading and supply information about potential therapeutic targets.

4.1. Limitations

Despite having the largest cohort of HGGs measured with 7T MRSI thus far, our data are still not sufficient for in-depth statistical analysis of our findings. A larger number of patients will be necessary. This will enable a more detailed evaluation of tumor ROIs and a comparison to established clinical imaging modalities like PET.

In order to reliably image gliomas in the basal parts of the brain, significant improvements in B_0 shim hardware is warranted to improve B_0 homogeneity throughout the brain (Juchem et al., 2020; Wilson et al., 2019). Together with motion correction, this will improve the robustness of 7T MRSI, particularly when whole-brain coverage is required (Maudsley et al., 2020).

Due to the short TR of 450 ms and the different T1s of metabolites, the results are affected by T1-weighting, but without knowledge of T1 relaxation times (i.e., this is particularly problematic in tumors and for low-abundant metabolites), corrections are not feasible. This prohibits the estimation of tissue concentrations, especially in tumors, but metabolic ratios could be explored as alternatives. Our limited simulations do explore the fitting precision of Gly and Gln, but should be expanded for a wider range of metabolites and situations in order to define the limits of quantification reliability more comprehensively.

There is evidence that the spectral pattern of the macromolecular background can vary in tumors. Despite promising results in healthy volunteers (Heckova et al., 2019; Považan et al., 2018), we could not reproduce these results in our patient population. Thus, we opted for a

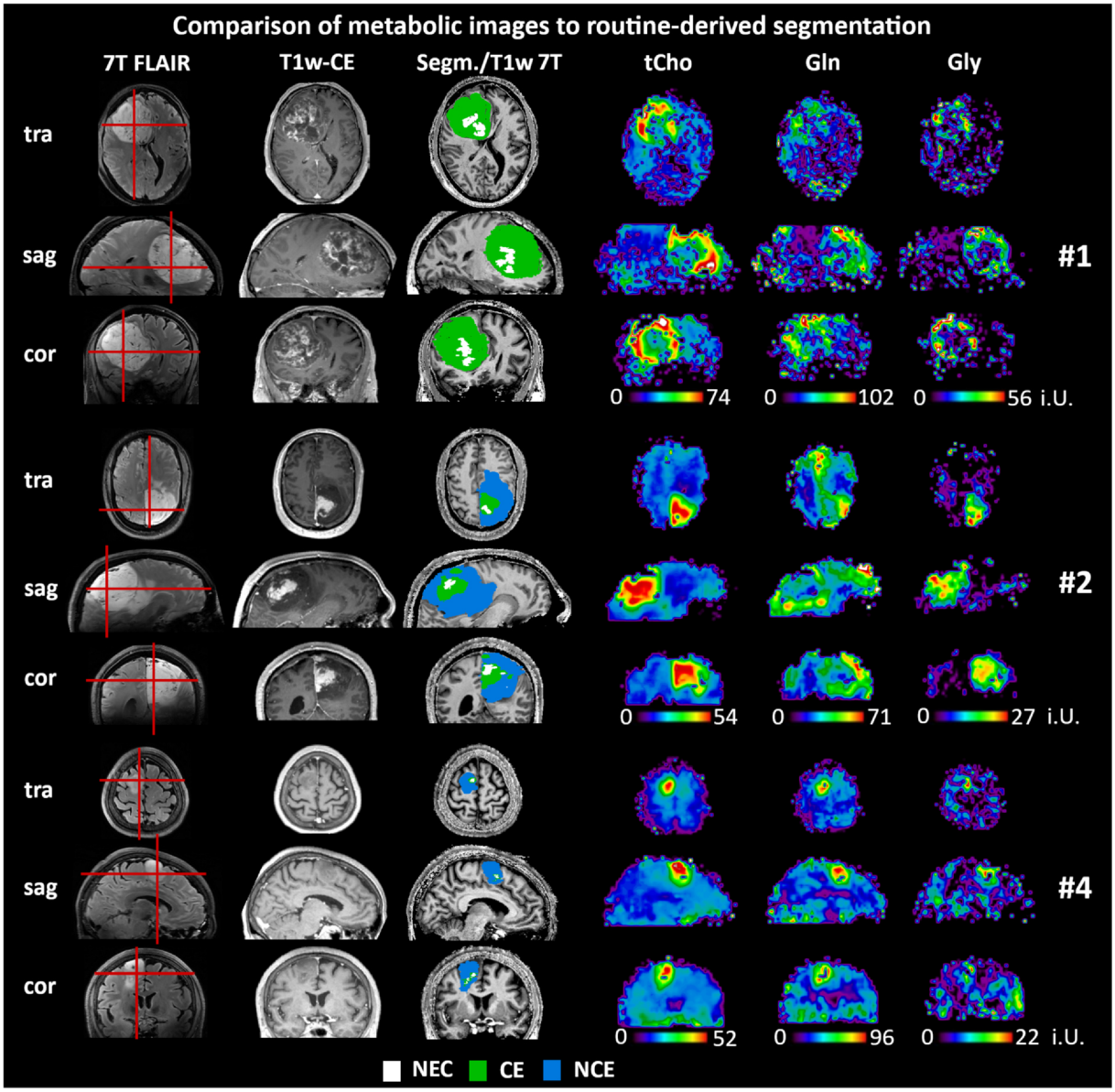

Fig. 5. Compared to a clinical imaging-derived segmentation, tCho, Gln, and Gly images have similar, but more differentiated hotspots which could lead to the development of metabolic regional profiles. The red reference lines indicate the positions of the displayed MRSI slices.

single MM contribution, which should be replaced by a more flexible parameterized MM model to account for changes in the spectral pattern of macromolecular components (Cudalbu et al., 2020). Lactate quantification is of major relevance for the mapping of the Warburg effect in brain tumors, but is currently not feasible with our whole-brain MRSI approach. Intratumoral lipid quantification (Delikatny et al., 2011) as well is not possible due to acquisition-based lipid artifacts and their removal. While successful quantification of 2HG as preoperative IDH-marker would be of high interest (Andronesi et al., 2018), reliable separation of 2HG and spectrally overlapping resonances appears challenging for FID-MRSI. However, our findings suggest that Glu, for which individual changes become visible after the separation of Gln at 7T, could be a surrogate marker for the absence of IDH-mutations. This should be investigated further, especially within a larger subject population and one that also includes low-grade gliomas that feature more frequent IDH mutations.

4.2. Outlook

The necessary next steps in the clinical evaluation of 7T FID-MRSI are the inclusion of a larger patient cohort and an investigation of the potential of specific metabolic markers such as Gln and Gly, for preoperative tumor margin delineation and grading, especially compared to the standard biomarker, tCho. The additional metabolic information provided by imaging the comprehensive neurochemical profile of brain tumors could have significant implications for radiomics and improve automatic segmentation of tumors based on mixed information from conventional MRI and metabolic imaging (Pedrosa de Barros et al., 2019). Improved preoperative localization via this new metabolic imaging method could translate to improved neurosurgical resection accuracy via a better characterization of the infiltration at the tumor border. Postoperative follow-ups, especially during radiation therapy, could improve the tracking of treatment success.

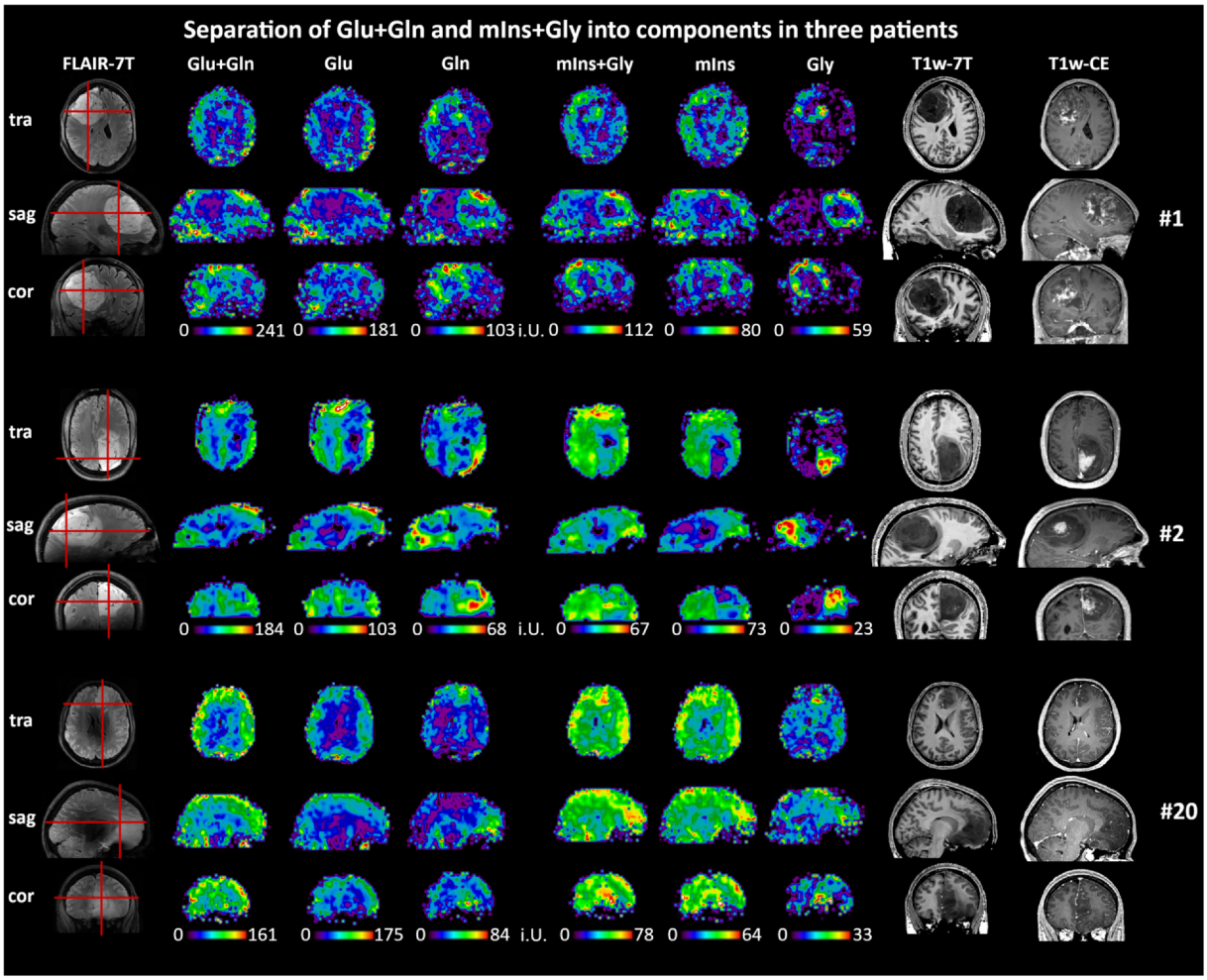

Fig. 6. A comparison of the Glu + Gln and mIns + Gly combined and separated shows the benefit of the 7T spectral resolution that enables the detection of metabolic alterations that would have remained inconspicuous on the sum images. In particular, the Gly hotspot in patient #2 is not apparent on the mIns + Gly image. The red reference lines indicate the positions of the displayed MRSI slices.

4.3. Conclusions

We successfully demonstrated fast high-resolution whole-brain 3D-MRSI at 7T in HGG patients, with the reliable quantification of ten metabolites, and clearly discernible structural metabolic differences between tumor and healthy-appearing tissues. Increases in tCho, Gln, and Gly corresponded very well to clinical tumor segmentation and showcase the potential of 7T MRSI to image Gln separated from Glu and Gly separated from mIns. In the future, this method could lead to a new quality of metabolic imaging in addition to the capabilities of current clinical MRI techniques that would improve the preoperative definition of tumor margins in high-grade gliomas.

CRediT authorship contribution statement

Gilbert Hangel: Conceptualization, Methodology, Validation, Investigation, Data curation, Writing - original draft, Visualization, Project administration, Funding acquisition. **Cornelius Cadrien:** Software, Formal analysis. **Philipp Lazen:** Software, Formal analysis, Investigation. **Julia Furtner:** Investigation, Data curation, Resources. **Alexandra Lipka:** Investigation. **Eva Hečková:** Investigation, Writing - review & editing. **Lukas Hingerl:** Software, Writing - review & editing. **Stanislav Motyka:** Software, Investigation. **Stephan Gruber:** Methodology, Writing - review & editing. **Bernhard Strasser:** Software, Writing - review & editing. **Barbara Kiesel:** Resources, Project administration. **Mario Mischkulnig:** Resources, Project administration. **Matthias Preusser:** Methodology, Writing - review & editing. **Thomas Roetzer:** Resources, Writing - review & editing, Funding acquisition. **Adelheid Wöhrer:** Resources, Writing - review & editing. **Georg Widhalm:** Conceptualization, Methodology, Resources, Supervision, Project administration. **Karl Rössler:** Resources, Writing - review & editing, Supervision. **Siegfried Trattnig:** Conceptualization, Writing - review & editing, Supervision, Funding acquisition. **Wolfgang Bogner:** Conceptualization, Methodology, Writing - review & editing, Supervision, Funding acquisition.

Declaration of Competing Interest

MP has received honoraria for lectures, consultation or advisory board participation from the following for-profit companies: Bayer, Bristol-Myers Squibb, Novartis, Gerson Lehrman Group (GLG), CMC Contrast, GlaxoSmithKline, Mundipharma, Roche, BMJ Journals, MedMedia, Astra Zeneca, AbbVie, Lilly, Medahead, Daiichi Sankyo, Sanofi, Merck Sharp & Dome, Tocagen. The following for-profit companies have supported clinical trials and contracted research conducted by MP with payments made to his institution: Böhringer-Ingelheim, Bristol-Myers Squibb, Roche, Daiichi Sankyo, Merck Sharp & Dome, Novocure, GlaxoSmithKline, AbbVie.

Acknowledgments

This work was supported by the Austrian Science Fund (FWF) grants KLI-646 and P 30701. TR is a recipient of a DOC Fellowship (25262) of the Austrian Academy of Sciences at the Division of Neuropathology and Neurochemistry, Department of Neurology, Medical University of Vienna.

Appendix A. Supplementary data

Supplementary data to this article can be found online at https://doi.org/10.1016/j.nicl.2020.102433.

References

Altman, B.J., Stine, Z.E., Dang, C.V., 2016. From Krebs to clinic: glutamine metabolism to cancer therapy. Nat. Rev. Cancer 16, 619–634. https://doi.org/10.1038/nrc.2016.71.

Andronesi, O.C., Arrillaga-Romany, I.C., Ly, K.I., Bogner, W., Ratai, E.M., Reitz, K., Iafrate, A.J., Dietrich, J., Gerstner, E.R., Chi, A.S., Rosen, B.R., Wen, P.Y., Cahill, D.P., Batchelor, T.T., 2018. Pharmacodynamics of mutant-IDH1 inhibitors in glioma patients probed by in vivo 3D MRS imaging of 2-hydroxyglutarate. Nat. Commun. 9, 1474. https://doi.org/10.1038/s41467-018-03905-6.

Berrington, A., Voets, N.L., Larkin, S.J., de Pennington, N., Mccullagh, J., Stacey, R., Schofield, C.J., Jezzard, P., Clare, S., Cadoux-Hudson, T., Plaha, P., Ansorge, O., Emir, U.E., 2018. A comparison of 2-hydroxyglutarate detection at 3 and 7 T with long-TE semi-LASER. NMR Biomed. 31, e3886. https://doi.org/10.1002/nbm.3886.

Bilgic, B., Chatnuntawech, I., Fan, A.P., Setsompop, K., Cauley, S.F., Wald, L.L., Adalsteinsson, E., 2013. Fast image reconstruction with L2-regularization. J. Magn. Reson. Imaging 00, 1–11. https://doi.org/10.1002/jmri.24365.

Bogner, W., Gruber, S., Trattnig, S., Chmelik, M., 2012. High-resolution mapping of human brain metabolites by free induction decay 1H MRSI at 7T. NMR Biomed. 25, 873–882. https://doi.org/10.1002/nbm.1805.

Bogner, W., Otazo, R., Henning, A., 2020. Accelerated MR spectroscopic imaging—a review of current and emerging techniques. NMR Biomed. https://doi.org/10.1002/nbm.4314.

Boonzaier, N.R., Larkin, T.J., Matys, T., van der Hoorn, A., Yan, J.-L., Price, S.J., 2017. Multiparametric MR imaging of diffusion and perfusion in contrast-enhancing and nonenhancing components in patients with glioblastoma. Radiology 284, 180–190. https://doi.org/10.1148/radiol.2017160150.

Branzoli, F., Deelchand, D.K., Sanson, M., Lehéricy, S., Marjańska, M., 2019. In vivo ^{1} H MRS detection of cystathionine in human brain tumors. Magn. Reson. Med. 82. https://doi.org/10.1002/mrm.27810.

Bulik, M., Jancalek, R., Vanicek, J., Skoch, A., Mechl, M., 2013. Potential of MR spectroscopy for assessment of glioma grading. Clin. Neurol. Neurosurg. 115, 146–153. https://doi.org/10.1016/j.clineuro.2012.11.002.

Caulo, M., Panara, V., Tortora, D., Mattei, P.A., Briganti, C., Pravatà, E., Salice, S., Cotroneo, A.R., Tartaro, A., 2014. Data-driven grading of brain gliomas: a multiparametric MR imaging study. Radiology 272, 494–503. https://doi.org/10.1148/radiol.14132040.

Choi, C., Dimitrov, I., Douglas, D., Zhao, C., Hawesa, H., Ghose, S., Tamminga, C.A., 2009. In vivo detection of serine in the human brain by proton magnetic resonance spectroscopy (1 H-MRS) at 7 Tesla. Magn. Reson. Med. 62, 1042–1046. https://doi.org/10.1002/mrm.22079.

Cudalbu, C., Behar, K.L., Bhattacharyya, P.K., Bogner, W., Borbath, T., Graaf, R.A. de, Gruetter, R., Henning, A., Juchem, C., Kreis, R., Lee, P., Lei, H., Marjańska, M., Mekle, R., Murali-Manohar, S., Považan, M., Rackayová, V., Wright*, A.M., Simicic, D., Slotboom, J., Jr., Z.S., Starčuková, J., Soher, B.J., Tkáč, I., Williams, S., Wilson, M., Xin, L., Mlynárik, V., 2020. Contribution of macromolecules to brain 1H MR spectra: Experts' consensus recommendations. NMR Biomed.

Delikatny, E.J., Chawla, S., Leung, D.-J., Poptani, H., 2011. MR-visible lipids and the tumor microenvironment. NMR Biomed. https://doi.org/10.1002/nbm.1661.

Fatou, B., Saudemont, P., Leblanc, E., Vinatier, D., Mesdag, V., Wisztorski, M., Focsa, C., Salzet, M., Ziskind, M., Fournier, I., 2016. In vivo Real-Time Mass Spectrometry for Guided Surgery Application. Sci. Reports 2016 6 6, 25919. DOI:10.1038/srep25919.

Ganji, S.K., Maher, E.A., Choi, C., 2016. In vivo 1 HMRSI of glycine in brain tumors at 3T. Magn. Reson. Med. 75, 52–62. https://doi.org/10.1002/mrm.25588.

Gruber, S., Heckova, E., Strasser, B., Považan, M., Hangel, G.J., Minarikova, L., Trattnig, S., Bogner, W., 2017. Mapping an extended neurochemical profile at 3 and 7 T using accelerated high-resolution proton magnetic resonance spectroscopic imaging. Invest. Radiol. 52. https://doi.org/10.1097/RLI.0000000000000379.

Hangel, G., Strasser, B., Považan, M., Heckova, E., Hingerl, L., Boubela, R., Gruber, S., Trattnig, S., Bogner, W., 2016. Ultra-high resolution brain metabolite mapping at 7 T by short-TR Hadamard-encoded FID-MRSI. Neuroimage 168, 199–210. https://doi.org/10.1016/j.neuroimage.2016.10.043.

Hangel, G., Jain, S., Springer, E., Hečková, E., Strasser, B., Považan, M., Gruber, S., Widhalm, G., Kiesel, B., Furtner, J., Preusser, M., Roetzer, T., Trattnig, S., Sima, D.M., Smeets, D., Bogner, W., 2019. High-resolution metabolic mapping of gliomas via patch-based super-resolution magnetic resonance spectroscopic imaging at 7T. Neuroimage 191, 587–595. https://doi.org/10.1016/j.neuroimage.2019.02.023.

Heckova, E., Považan, M., Strasser, B., Motyka, S., Hangel, G., Hingerl, L., Moser, P., Lipka, A., Gruber, S., Trattnig, S., Bogner, W., 2019. Effects of different macromolecular models on reproducibility of FID-MRSI at 7T. Magn. Reson. Med. https://doi.org/10.1002/mrm.27922.

Henning, A., Fuchs, A., Murdoch, J.B., Boesiger, P., 2009. Slice-selective FID acquisition, localized by outer volume suppression (FIDLOVS) for ^{1}H-MRSI of the human brain at 7 T with minimal signal loss. NMR Biomed. 22, 683–696. https://doi.org/10.1002/nbm.1366.

Hingerl, L., Bogner, W., Moser, P., Považan, M., Hangel, G., Heckova, E., Gruber, S., Trattnig, S., Strasser, B., 2018. Density-weighted concentric circle trajectories for high resolution brain magnetic resonance spectroscopic imaging at 7T. Magn. Reson. Med. 79, 2874–2885. https://doi.org/10.1002/mrm.26987.

Hingerl, L., Strasser, B., Moser, P., Hangel, G., Motyka, S., Heckova, E., Gruber, S., Trattnig, S., Bogner, W., 2019. Clinical high-resolution 3D-MR spectroscopic imaging of the human brain at 7 T. Invest. Radiol. 1. https://doi.org/10.1097/RLI.0000000000000626.

Juchem, C., Cudalbu, C., de Graaf, R.A., Gruetter, R., Henning, A., Hetherington, H.P., Boer, V.O., 2020. B0 shimming for in vivo magnetic resonance spectroscopy: experts' consensus recommendations. NMR Biomed accepted.

Kallenberg, K., Bock, H.C., Helms, G., Jung, K., Wrede, A., Buhk, J.-H., Giese, A., Frahm, J., Strik, H., Dechent, P., Knauth, M., 2009. Untreated glioblastoma multiforme: increased myo -inositol and glutamine levels in the contralateral cerebral hemisphere at proton MR spectroscopy. Radiology 253, 805–812. https://doi.org/10.1148/radiol.2533071654.

Kim, D., Fiske, B.P., Birsoy, K., Freinkman, E., Kami, K., Possemato, R.L., Chudnovsky, Y., Pacold, M.E., Chen, W.W., Cantor, J.R., Shelton, L.M., Gui, D.Y., Kwon, M., Ramkissoon, S.H., Ligon, K.L., Kang, S.W., Snuderl, M., Vander Heiden, M.G., Sabatini, D.M., 2015. SHMT2 drives glioma cell survival in ischaemia but imposes a dependence on glycine clearance. Nature 520, 363–367. https://doi.org/10.1038/nature14363.

Lei, H., Peeling, J., 2000. Simultaneous spectral editing for γ-aminobutyric acid and taurine using double quantum coherence transfer. J. Magn. Reson. 143, 95–100. https://doi.org/10.1006/jmre.1999.1958.

Li, Y., Larson, P., Chen, A.P., Lupo, J.M., Ozhinsky, E., Kelley, D., Chang, S.M., Nelson, S.J., 2015. Short-echo three-dimensional H-1 MR spectroscopic imaging of patients with glioma at 7 tesla for characterization of differences in metabolite levels. J. Magn. Reson. Imaging 41, 1332–1341. https://doi.org/10.1002/jmri.24672.

Louis, D.N., Perry, A., Reifenberger, G., von Deimling, A., Figarella-Branger, D., Cavenee, W.K., Ohgaki, H., Wiestler, O.D., Kleihues, P., Ellison, D.W., 2016. The 2016 World Health Organization classification of tumors of the central nervous system: a summary. Acta Neuropathol. 131, 803–820. https://doi.org/10.1007/s00401-016-1545-1.

Mattaini, K.R., Sullivan, M.R., Vander Heiden, M.G., 2016. The importance of serine metabolism in cancer. J. Cell Biol. 214, 249–257. https://doi.org/10.1083/jcb.201604085.

Maudsley, A.A., Domenig, C., Govind, V., Darkazanli, A., Studholme, C., Arheart, K., Bloomer, C., 2009. Mapping of brain metabolite distributions by volumetric proton MR spectroscopic imaging (MRSI). Magn. Reson. Med. 61, 548–559. https://doi.org/10.1002/mrm.21875.

Maudsley, A.A., Gupta, R.K., Stoyanova, R., Parra, N.A., Roy, B., Sheriff, S., Hussain, N., Behari, S., 2014. Mapping of glycine distributions in gliomas. AJNR. Am. J. Neuroradiol. 35, S31–S36. https://doi.org/10.3174/ajnr.A3845.

Maudsley, A.A., Andronesi, O.C., Barker, P.B., Bizzi, A., Bogner, W., Henning, A., Nelson, S.J., Posse, S., Shungu, D.C., Soher, B.J., 2020. Advanced magnetic resonance spectroscopic neuroimaging: experts' consensus recommendations. NMR Biomed. https://doi.org/10.1002/nbm.4309.

McBean, G.J., 2017. Cysteine, glutathione, and thiol redox balance in astrocytes. Antioxidants (Basel, Switzerland) 6. https://doi.org/10.3390/antiox6030062.

Mert, A., Kiesel, B., Wöhrer, A., Martínez-Moreno, M., Minchev, G., Furtner, J., Knosp, E., Wolfsberger, S., Widhalm, G., 2015. Introduction of a standardized multimodality image protocol for navigation-guided surgery of suspected low-grade gliomas. Neurosurg. Focus 38, E4. https://doi.org/10.3171/2014.10.FOCUS14597.

Mörén, L., Tommy Bergenheim, A., Ghasimi, S., Brännström, T., Johansson, M., Antti, H., 2015. Metabolomic screening of tumor tissue and serum in glioma patients reveals diagnostic and prognostic information. Metabolites 5, 502–520. https://doi.org/10.3390/metabo5030502.

Moser, P., Bogner, W., Hingerl, L., Heckova, E., Hangel, G., Motyka, S., Trattnig, S., Strasser, B., 2019. Non-Cartesian GRAPPA and coil combination using interleaved calibration data – application to concentric-ring MRSI of the human brain at 7T. Magn. Reson. Med. 82, 1587–1603. https://doi.org/10.1002/mrm.27822.

Moser, E., Stahlberg, F., Ladd, M.E., Trattnig, S., 2012. 7-T MR-from research to clinical applications? NMR Biomed. 25, 695–716. https://doi.org/10.1002/nbm.1794.

Obara-Michlewska, M., Szeliga, M., 2020. Targeting glutamine addiction in gliomas. Cancers (Basel) 12, 310. https://doi.org/10.3390/cancers12020310.

Ogg, R.J., Kingsley, P.B., Taylor, J.S., 1994. WET, a T1- and B1-insensitive water-suppression method for in vivo localized 1H NMR spectroscopy. J. Magn. Reson. B 104, 1–10. https://doi.org/10.1006/jmrb.1994.1048.

Pedrosa de Barros, N., Meier, R., Pletscher, M., Stettler, S., Knecht, U., Reyes, M., Gralla, J., Wiest, R., Slotboom, J., 2019. Analysis of metabolic abnormalities in high-grade glioma using MRSI and convex NMF. NMR Biomed. https://doi.org/10.1002/nbm.4109.

Potter, M., Newport, E., Morten, K.J., 2016. The Warburg effect: 80 years on. Biochem. Soc. Trans. 44, 1499–1505. https://doi.org/10.1042/BST20160094.

Považan, M., Strasser, B., Hangel, G., Chmelík, M., Gruber, S., Trattnig, S., Bogner, W., 2014. Automated routine for MRSI data processing. In: 2nd TRANSACT Meeting – Quality Issues in Clinical MR Spectroscopy. University and Inselspital Bern, Switzerland, pp. S2.

Považan, M., Hangel, G., Strasser, B., Gruber, S., Chmelik, M., Trattnig, S., Bogner, W., 2015. Mapping of brain macromolecules and their use for spectral processing of < sup > 1 < /sup > H-MRSI data with an ultra-short acquisition delay at 7T. Neuroimage 121. https://doi.org/10.1016/j.neuroimage.2015.07.042.

Považan, M., Strasser, B., Hangel, G., Heckova, E., Gruber, S., Trattnig, S., Bogner, W., 2018. Simultaneous mapping of metabolites and individual macromolecular components via ultra-short acquisition delay 1 H MRSI in the brain at 7T. Magn. Reson. Med. 79, 1231–1240. https://doi.org/10.1002/mrm.26778.

Righi, V., Andronesi, O.C., Mintzopoulos, D., Black, P.M., Tzika, A.A., 2010. High-resolution magic angle spinning magnetic resonance spectroscopy detects glycine as a biomarker in brain tumors. Int. J. Oncol. 36, 301–306. https://doi.org/10.3892/ijo_00000500.

Stadlbauer, A., Nimsky, C., Buslei, R., Pinker, K., Gruber, S., Hammen, T., Buchfelder, M., Ganslandt, O., 2007. Proton magnetic resonance spectroscopic imaging in the border zone of gliomas: correlation of metabolic and histological changes at low tumor infiltration–initial results. Invest. Radiol. 42, 218–223. https://doi.org/10.1097/01.rli.0000255812.61435.67.

Stadlbauer, A., Zimmermann, M., Doerfler, A., Oberndorfer, S., Buchfelder, M., Coras, R., Kitzwögerer, M., Roessler, K., 2018. Intratumoral heterogeneity of oxygen metabolism and neovascularization uncovers 2 survival-relevant subgroups of IDH1 wild-type glioblastoma. Neuro. Oncol. 20, 1536–1546. https://doi.org/10.1093/neuonc/noy066.

St-Arnaud, K., Aubertin, K., Strupler, M., Madore, W.-J., Grosset, A.-A., Petrecca, K., Trudel, D., Leblond, F., 2018. Development and characterization of a handheld hyperspectral Raman imaging probe system for molecular characterization of tissue on mesoscopic scales. Med. Phys. 45, 328–339. https://doi.org/10.1002/mp.12657.

Strasser, B., Chmelik, M., Robinson, S.D., Hangel, G., Gruber, S., Trattnig, S., Bogner, W., 2013. Coil combination of multichannel MRSI data at 7 T: MUSICAL. NMR Biomed. 26, 1796–1805. https://doi.org/10.1002/nbm.3019.

Strasser, B., Považan, M., Hangel, G., Hingerl, L., Chmelik, M., Gruber, S., Trattnig, S., Bogner, W., 2017. (2 + 1)D-CAIPIRINHA accelerated MR spectroscopic imaging of the brain at 7T. Magn. Reson. Med. 78, 429–440. https://doi.org/10.1002/mrm.26386.

Tanaka, K., Sasayama, T., Irino, Y., Takata, K., Nagashima, H., Satoh, N., Kyotani, K., Mizowaki, T., Imahori, T., Ejima, Y., Masui, K., Gini, B., Yang, H., Hosoda, K., Sasaki, R., Mischel, P.S., Kohmura, E., 2015. Compensatory glutamine metabolism promotes glioblastoma resistance to mTOR inhibitor treatment. J. Clin. Invest. 125, 1591–1602. https://doi.org/10.1172/JCI78239.

Venkataramani, V., Tanev, D.I., Strahle, C., Studier-Fischer, A., Fankhauser, L., Kessler, T., Körber, C., Kardorff, M., Ratliff, M., Xie, R., Horstmann, H., Messer, M., Paik, S.P., Knabbe, J., Sahm, F., Kurz, F.T., Acikgöz, A.A., Herrmannsdörfer, F., Agarwal, A., Bergles, D.E., Chalmers, A., Miletic, H., Turcan, S., Mawrin, C., Hänggi, D., Liu, H.-K., Wick, W., Winkler, F., Kuner, T., 2019. Glutamatergic synaptic input to glioma cells drives brain tumour progression. Nature 573, 532–538. https://doi.org/10.1038/s41586-019-1564-x.

Wang, Q., Zhang, H., Zhang, J., Wu, C., Zhu, W., Li, F., Chen, X., Xu, B., 2016. The diagnostic performance of magnetic resonance spectroscopy in differentiating high-from low-grade gliomas: a systematic review and meta-analysis. Eur. Radiol. 26, 2670–2684. https://doi.org/10.1007/s00330-015-4046-z.

Wilson, M., Andronesi, O., Barker, P.B., Bartha, R., Bizzi, A., Bolan, P.J., Brindle, K.M., Choi, I., Cudalbu, C., Dydak, U., Emir, U.E., Gonzalez, R.G., Gruber, S., Gruetter, R., Gupta, R.K., Heerschap, A., Henning, A., Hetherington, H.P., Huppi, P.S., Hurd, R.E., Kantarci, K., Kauppinen, R.A., Klomp, D.W.J., Kreis, R., Kruiskamp, M.J., Leach, M.O., Lin, A.P., Luijten, P.R., Marjańska, M., Maudsley, A.A., Meyerhoff, D.J., Mountford, C.E., Mullins, P.G., Murdoch, J.B., Nelson, S.J., Noeske, R., Öz, G., Pan, J.W., Peet, A.C., Poptani, H., Posse, S., Ratai, E., Salibi, N., Scheenen, T.W.J., Smith, I.C.P., Soher, B.J., Tkáč, I., Vigneron, D.B., Howe, F.A., 2019. Methodological consensus on clinical proton MRS of the brain: review and recommendations. Magn. Reson. Med. 82, 527–550. https://doi.org/10.1002/mrm.27742.

Wise, D.R., Ward, P.S., Shay, J.E.S., Cross, J.R., Gruber, J.J., Sachdeva, U.M., Platt, J.M., DeMatteo, R.G., Simon, M.C., Thompson, C.B., 2011. Hypoxia promotes isocitrate dehydrogenase-dependent carboxylation of -ketoglutarate to citrate to support cell growth and viability. Proc. Natl. Acad. Sci. 108, 19611–19616. https://doi.org/10.1073/pnas.1117773108.

Yan, H., Parsons, D.W., Jin, G., McLendon, R., Rasheed, B.A., Yuan, W., Kos, I., Batinic-Haberle, I., Jones, S., Riggins, G.J., Friedman, H., Friedman, A., Reardon, D., Herndon, J., Kinzler, K.W., Velculescu, V.E., Vogelstein, B., Bigner, D.D., 2009. *IDH1* and *IDH2* Mutations in Gliomas. N. Engl. J. Med. 360, 765–773. https://doi.org/10.1056/NEJMoa0808710.